Nano Select

WILEY-VCH

RESEARCH ARTICLE OPEN ACCESS

Green Synthesis of Silver Nanoparticles With *Cyclosorus dentatus* and *Nephrolepis biserrata* and Their Antioxidant, Anti-Inflammatory Studies

Christian Nanga Chick[1,2] | Francois Eya'ane Meva[2,3] | Phillippe Belle Ebanda Kedi[2,4] | Toyonobu Usuki[1]

[1]Department of Materials and Life Sciences, Faculty of Science and Technology, Sophia University, Chiyoda-ku, Tokyo, Japan | [2]Laboratory of Innovative Nanostructured Material (NANO: C), Faculty of Medicine and Pharmaceutical Sciences, The University of Douala, Douala, Cameroon | [3]Institute for Organic Chemistry and Structural Chemistry, Heinrich-Heine-University Dusseldorf, Dusseldorf, Germany | [4]Nanosciences African Network, iThemba LABS-National Research Foundation, Cape Town, South Africa

Correspondence: Francois Eya'ane Meva (mevae@daad-alumni.de) | Toyonobu Usuki (t-usuki@sophia.ac.jp)

Received: 27 May 2024 | **Revised:** 7 July 2024 | **Accepted:** 8 July 2024

Funding: The authors received no specific funding for this work.

Keywords: antioxidant | *Cyclosorus dentatus* | IR | *Nephrolepis biserrata* | SNPs | UV-Vis

ABSTRACT

This study examined the synthesis of silver nanoparticles (SNPs) with aqueous extracts of *Cyclosorus dentatus* and *Nephrolepis biserrata* fronds and the evaluation of their biological activities. Mixing of $AgNO_3$ solution and the aqueous extracts resulted in color change, indicating the formation of SNPs. UV-Vis spectroscopy analysis gave a surface plasmon resonance (SPR) peak at approximately 420 nm, confirming the presence of the synthesized SNPs. Infrared analysis showed C-O, N-O, and C-C vibrations or stretching and aliphatic vibrations of hydrocarbon chains of the synthesized SNPs. x-Ray diffraction (XRD) analysis indicated the SNPs were face-centered, cubic, and crystalline in nature, with crystallite sizes. The scanning electron microscopy (SEM) shows the aggregation of the spherical shape nanoparticles. The SNPs significantly reduced phosphomolybdenum and captured H_2O_2 with respective IC_{50} values of 61.55 and 29.03 µg/mL for *C. dentatus* SNP (SNP-Cd), and 92.61 and 9.07 µg/mL for *N. biserrata* SNP (SNP-Nb), respectively. In terms of albumin-denaturing activity, the SNPs gave an IC_{50} value of 21.20 µg/mL for SNP-Cd and 7.18 µg/mL for SNP-Nb. Thus, this work confirmed that SNP-Cd and SNP-Nb are potential therapeutic agents for treating oxidative stress, inflammatory problems, and related diseases.

1 | Introduction

Pteridophytes (ferns and their allies) have evolutionarily succeeded and survived for a very long period, and they have a remarkable history of withstanding various harsh climatic and topographic conditions as compared to other plants. Globally, only a few percent of ferns have been studied for their medicinal values and properties [1, 2]. Applications of ferns include as sources of food and biofertilizers, ornamental plants, phytoremediators, and ethnomedicine components in humans and animals. Due to the limited scientific attention and investigation given to ferns, much of their potential medicinal and therapeutic values remain unknown.

The fern *Cyclosorus dentatus* belongs to the family Thelypteridacea and is commonly called the "downy maiden fern." Very little to no scientific findings are known about the secondary metabolites and bioactivities of this fern. A few parts of *C. dentatus* are used in a patent Chinese medicinal product for treating tympanites. Accumulation of antimony and antioxidative

This is an open access article under the terms of the Creative Commons Attribution License, which permits use, distribution and reproduction in any medium, provided the original work is properly cited.

© 2024 The Author(s). *Nano Select* published by Wiley-VCH GmbH.

activities has been reported for this fern [3]. The fern *Nephrolepis biserrata* belongs to the family Nephrolepidaceae and is commonly called the "giant sword fern." Medicinally, these ferns help with stomach problems and the treatment of wounds and blisters [4]. They are sources of flavonoids (myricetin, rutin, kaempferol), proteins, and phenolics [5]. Antihypertensive and anti-inflammatory activities, cytotoxic potential, glucosidase inhibitory effects, and antioxidant, chemopreventive, and antibacterial activities of solvent extracts of these ferns are reported [3–5].

As reported in some review articles, the past decades have witnessed tremendous advancement in green sciences, with one focus on nanotechnology directed toward biological synthesis using natural sources (plants or plant parts, bacteria, and fungi) that are more eco-friendly [6, 7]. Researchers are intensively screening for molecules that can reduce metallic ions to zerovalent atoms. Silver nanoparticles (SNPs) are among the most vital and fascinating metallic nanomaterials and have a variety of biomedical applications. Advantages of SNPs include their excellent electrical conductivity, chemical stability, and catalytic, antimicrobial, and cytotoxic activities. Moreover, plants and ferns, for example, *Microsorum pteropus*, and *Odontonema strictum*, have been investigated as promising biological nanomaterials [8, 9].

Regardless of the numerous benefits of the green approach, some shortcomings need to be considered for acquiring a consistent and uniform nanoparticle. The physicochemical and bioactivities of nanoparticles vary due to their differences in bioactive compounds; therefore, the chemical analysis of plant samples is very important. Recently, SNPs have been synthesized from the leaves of *Contoneaster nummularai*, olive fruit extracts, with respective diameter sizes of 121 and 77 nm having activities against various infectious agents with other functionalities [10, 11].

The present study is to examine the application of *C. dentatus* and *N. biserrata* aqueous extracts to the synthesis of SNPs for the first time. The SNPs were physically characterized, and the in vitro antioxidant and anti-inflammatory activities of the SNPs were assessed to evaluate their potential pharmacological applications.

2 | Results and Discussion

C. dentatus (*Forsk*.) Ching. L. (Figure S1) and *N. biserrate* (*Sw*.) Schott (Figure S2) ferns were collected at Bonaberi, Littoral region, Cameroon. The verification and taxonomic coverage of the ferns were carried out at the National Herbarium of Cameroon, Yaounde, and the pteridophytes were obtained per voucher specimens with herbarium numbers 21182/SRF/Cam and 17798/SRF/Cam, respectively. Fine cuts of 10 g in weight of each fern are macerated in 100 mL of preheated distilled water (80°C) and stirred for 5 min [12]. A total of 10 mL of each aqueous extract was added to 50 mL of $AgNO_3$ solution (1 mM) and incubated in the dark at room temperature to minimize photoactivation of the $AgNO_3$ [13]. Next, color changes and UV-Vis spectroscopy measurements were carried out at regular intervals for 2 days. The prepared SNP solutions were centrifuged

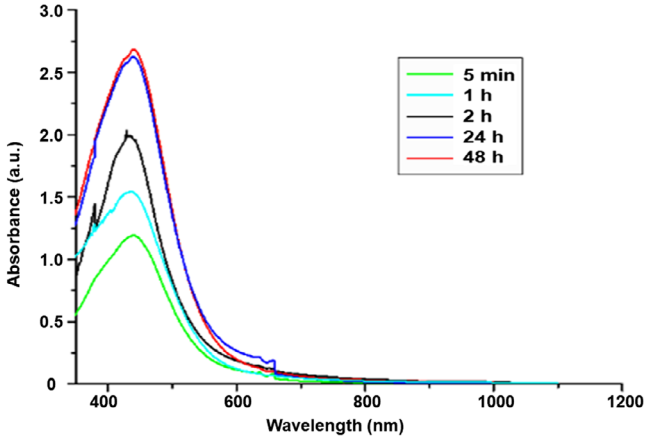


FIGURE 1 | UV-Vis spectra of SNP-Cd at different incubation times. SNP-Cd, *C. dentatus* SNP.

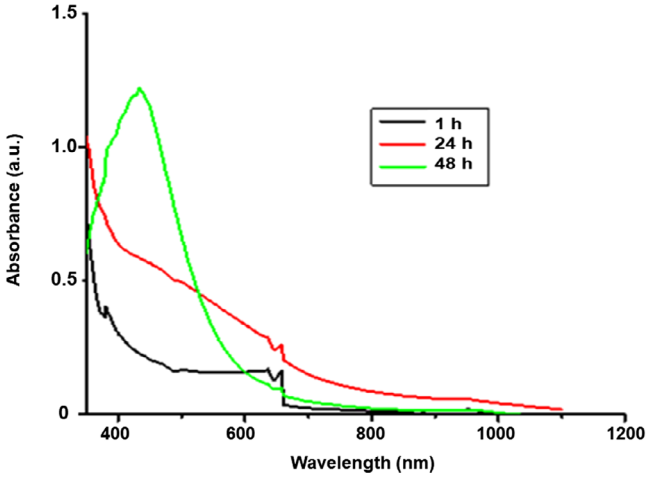


FIGURE 2 | UV-Vis spectra of SNP-Nb at different incubation times. SNP-Nb, *N. biserrata* SNP.

at 6000 rpm for 20 min, and the SNPs were then washed with distilled H_2O. The obtained pellets and supernatants were placed on petri dishes, dried in an oven at 60°C for 1 day, and then used for further investigations.

The observed color of the SNP solutions changed from light green or yellow to dark brown (C) after the addition of $AgNO_3$ solution (A) or aqueous extract solution (B), as demonstrated in Figures S3–S4. The color change indicated the formation of reduced SNPs after incubation for 48 h. The color of the *C. dentatus* SNP (SNP-Cd) solution changed more rapidly than that of the *N. biserrata* SNP (SNP-Nb) solution. No significant color changes occurred by the third day of incubation.

UV-Vis spectra of synthesized SNPs monitored at different time intervals are shown in Figures 1 and 2. The prepared SNPs samples measured at time $t = 0$ were not recorded because no peak was observed. A localized surface plasmon resonance (LSPR) peak at approximately 420 nm formed after 5 min of incubation for the SNP-Cd solution, markedly earlier than the peak formed for the SNP-Nb solution, in which the SPR peak was observed after 48 h of incubation. For SNP-Cd following

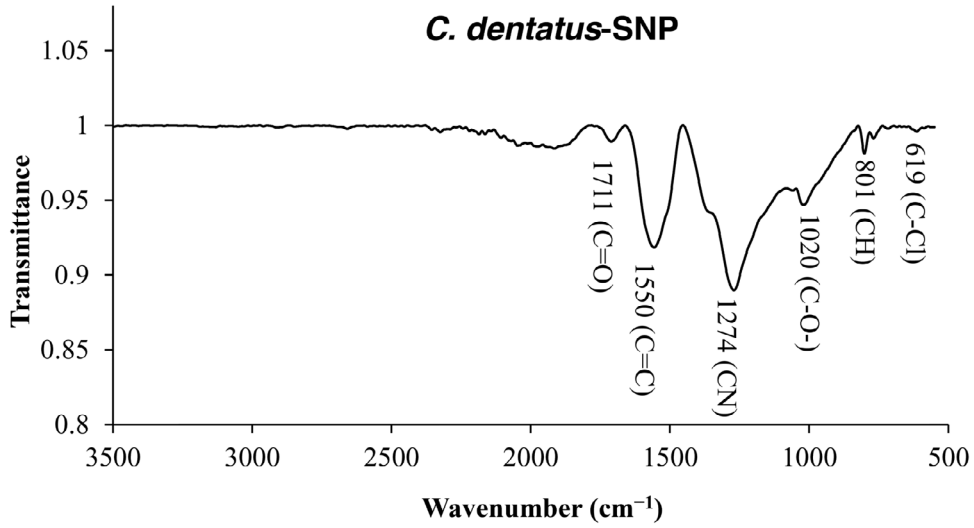


FIGURE 3 | IR spectra of SNP-Cd. IR, infrared; SNP-Cd, *C. dentatus* SNP.

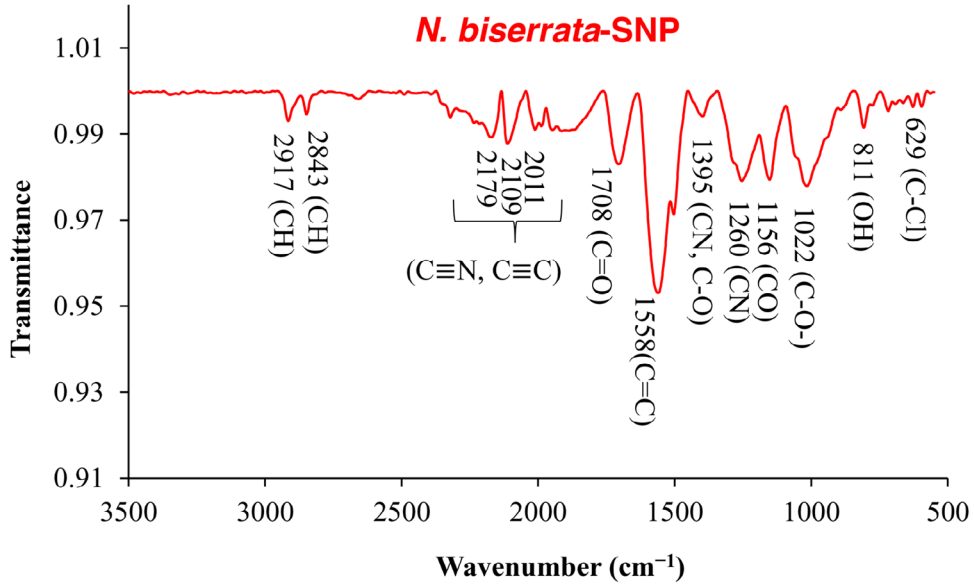


FIGURE 4 | IR spectra of SNP-Nb. IR, infrared; SNP-Nb, *N. biserrata* SNP.

the passage of time, an increase in wavelength was observed with a simultaneous red shift indicating aggregation of the nanoparticles.

The infrared (IR) spectra of the synthesized SNPs between 3500 and 500 cm^{-1} are established. Intense absorption bands at 1711, 1550, 1274, 1020, 801, and 619 cm^{-1} for SNP-Cd (Figure 3), and at 2840, 2910, 2011, 2109, 2179, 1708, 1558, 1395, 1260, 1156, 1022, 811, and 629 cm^{-1} for SNP-Nb (Figure 4) are observed, respectively.

For the spectral of SNP-Nb only, the absorption bands at 2910 and 2840 cm^{-1} are characteristic of the stretching vibration of methyl groups [14]. The weak bands between 2400 and 2000 cm^{-1} would be derived from the nitriles and alkyne functional moiety of the biomaterial. The absorption bands at 1395 cm^{-1} could be assigned to CN or C-O of phenol groups, and at the peak 1156 cm^{-1} for C-O bending [15].

For the spectral of both SNP-Cd and SNP-Nb, the carboxylic group for the conjugate aldehydes or a primary amide were present at 1711 and 1708 cm^{-1}. The C═C stretching at 1550 and 1558 cm^{-1} confirms the presence of an aromatic ring [16]. The bands at 1020 and 1022 cm^{-1} could be originated from the C-O vibration or the ether linkage, suggesting the presence of flavones [9, 11]. The bands observed at 801 and 811 cm^{-1} correspond to the out-of-plane bending vibration of the OH group. The appearance of the peak at 619 and 629 cm^{-1} could be related to O—Ag interaction in the produced nanoparticles, the C—Cl stretching in an alkyl group, or the out-of-plane bending vibration of the CH group [11, 17]. The absorption peaks indicate the elements or functional groups of the secondary metabolites from the aqueous extracts of *C. dentatus* and *N. biserrata* that are responsible for the reduction and capping or stabilization of the formed SNPs. Thus, a variety of compounds in the ferns *C. dentatus* and *N. biserrata* is involved in the synthesis of their respective SNPs.

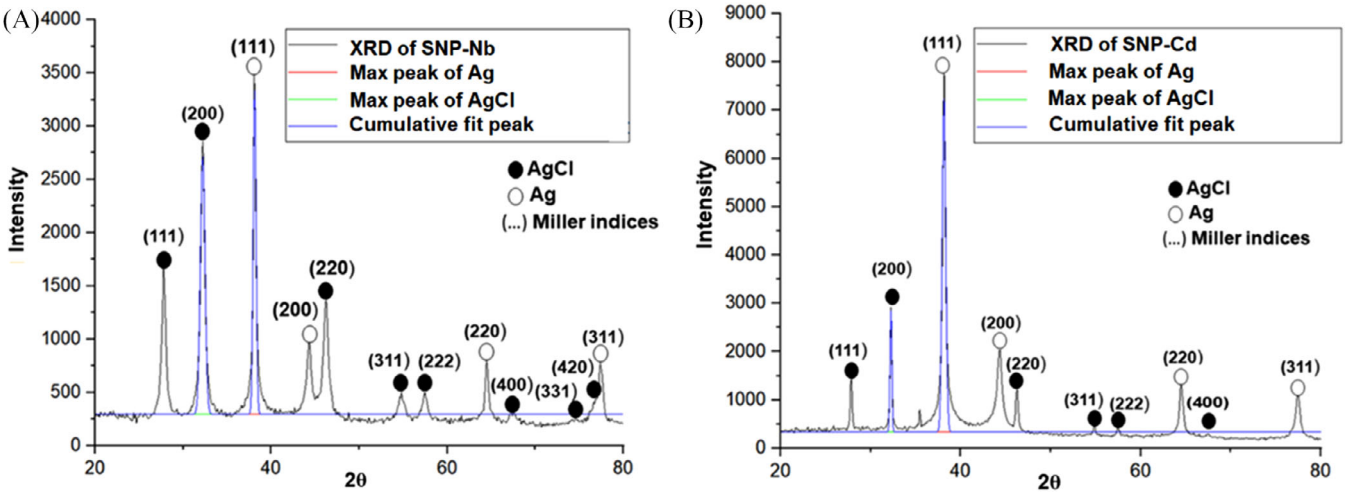


FIGURE 5 | Powder x-ray diffractograms of (A) SNP-Nb and (B) SNP-Cd. SNP-Cd, *C. dentatus* SNP; SNP-Nb, *N. biserrata* SNP.

Powder x-ray diffraction (XRD) patterns of SNP-Cd and SNP-Nb were also measured. The principal characteristic data and Rietveld refinement pattern graphics are shown in Figure 5 and along with Tables S1–S2 and Figures S6–S7, respectively. The plotted 2θ range was 20°–80°, and the diffractograms were compared with the standard powder diffraction cards of the Joint Committee of Powder Diffraction Standards under file numbers <65-2871> for Ag and <31-1238> for AgCl, as illustrated in Figures 5. The cubic phase of Ag for *C. dentatus* at diffraction point 2θ values of 38.08°, 44.25°, 64.42°, and 77.36° was indexed to (111), (200), (220), and (311) planes of the face-centered cubic structure, respectively. As shown in Figure 5, the cubic phase of AgCl of *C. dentatus* at diffraction point 2θ values of 27.77°, 32.18°, 46.17°, 54.74°, 57.37°, and 67.32° was indexed to (111), (200), (220), (311), (222), and (400) planes, respectively. The cubic phase of Ag for *N. biserrata* at diffraction point 2θ values of 38.09°, 44.25°, 64.43°, and 77.36° was indexed to (111), (200), (220), and (311) planes of the face-centered cubic structure, respectively. Finally, the cubic phase of AgCl for *N. biserrata* at diffraction point 2θ values of 27.77°, 32.19°, 46.18°, 54.74°, 57.38°, 67.34°, 74.31°, and 76.63° was indexed to (111), (200), (220), (311), (222), (400), (331), and (420) planes, respectively.

The average crystallite size (D) of the nanoparticles was calculated using the most intense peaks of Ag and AgCl. From the Scherrer formula, $D = 0.9\lambda/\beta\text{Cos}\theta$, where λ is the wavelength of the x-ray used for diffraction and β is the full width at half maximum (FWHM) of the peak representing the cumulative fit of the Gaussian function calculated using Origin software (Figure S8). The crystalline sizes for Ag and AgCl for the SNPs were calculated in Table S3. However, no additional significant Ag or AgCl peaks were observed on the diffractograms for SNP-Cd and SNP-Nb.

Scanning electron microscopy (SEM) was analyzed for SNP-Nb only. Spherical aggregates of different sizes were observed with a mean (SE) diameter of 149 ± 4.3 nm as shown in Figure 6. The energy dispersive x-ray spectroscopy (EDS) showed the elemental composition of SNP-Nb, as illustrated in Figure S9. The EDS absorption peaks at 2.6 and 3 keV, corresponding to Cl and Ag, were in good agreement with other reports [8, 9]. The peaks at 0.2 and 0.5 keV, corresponding to C and O, may be derived from

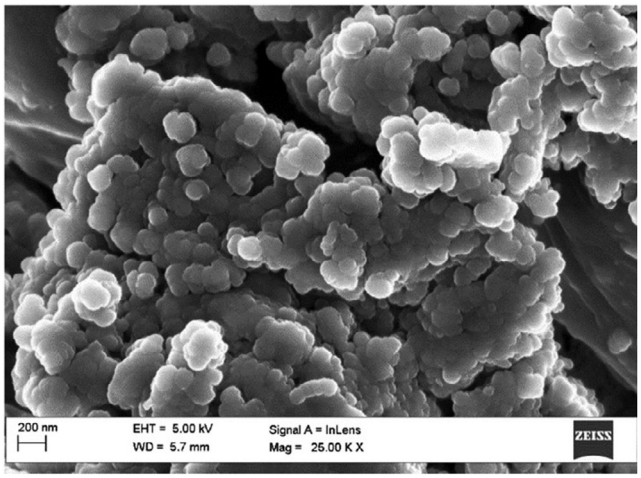


FIGURE 6 | SEM image of SNP-Nb. SEM, scanning electron microscopy; SNP-Nb, *N. biserrata* SNP.

compounds involved in SNP formation or from the sample grid holder, which was manufactured from carbon.

Dynamic light scattering (DLS) measurements indicated that the hydrodynamic particle size of SNP-Nb was 65.16 nm, and the polydispersive index was 0.415, indicating that the samples were suitable for analysis, as demonstrated in Figure 7. The hydrodynamic particle size was larger than the XRD crystallite size calculated using the Scherrer formula.

Antioxidant activity was then examined using the phosphomolybdenum reduction test according to the reported method [18]. In principle, this assay measures the ability of SNPs solutions synthesized from the mixture of the plant extracts and $AgNO_3$ solution (prepared in triplicate serial dilutions from 100 to 6.25 μg/mL) to reduce Mo(VI) to Mo(V). This reaction occurs in an acidic environment to form green-blue complexes of reduced phosphomolybdenum, as monitored by UV-Vis spectrophotometry at 695 nm. Equation (S1) shows the formula for calculating the percentage of reduced phosphomolybdenum. The percent inhibition of phosphomolybdenum reduction was directly

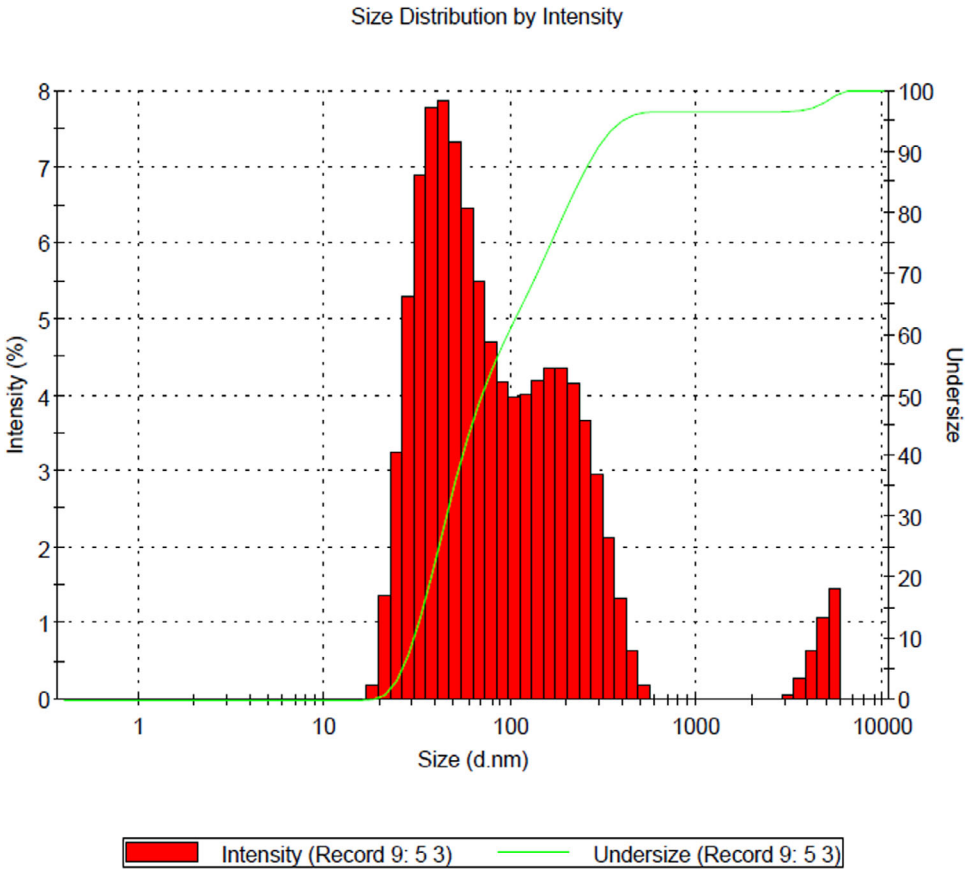


FIGURE 7 | DLS size distribution by intensity of SNP-Nb. DLS, dynamic light scattering; SNP-Nb, *C. dentatus* SNP.

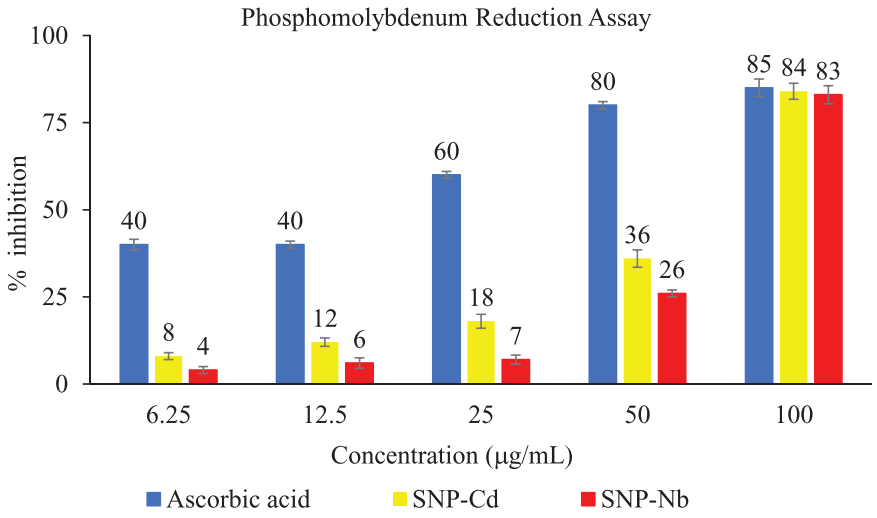


FIGURE 8 | Phosphomolybdenum reduction assay for SNP-Cd and SNP-Nb. SNP-Cd, *C. dentatus* SNP; SNP-Nb, *C. dentatus* SNP.

proportional to the quantity of SNPs tested, as shown in Figure 8. The maximum percent inhibition of phosphomolybdenum reduction was 84% for SNP-Cd and 83% for SNP-Nb at a concentration of 100 µg/mL. The IC_{50} calculation was the same as that reported in a previous work [8]. The IC_{50} was 61.55 µg/mL for SNP-Cd and 92.61 µg/mL for SNP-Nb. The positive reference ascorbic acid gave an IC_{50} value of 13.91 µg/mL. These results were dose dependent, and the differences were significant ($p < 0.05$).

The H_2O_2 scavenging method used in this study was the same as described in previous reports [8, 9]. The degree of H_2O_2 scavenging increased with increasing quantity of SNPs (Figure 9). This assay measures the ability of SNPs prepared in triplicate serial dilutions (100–6.25 µg/mL) to capture H_2O_2, as monitored by UV-Vis spectroscopy at a wavelength of 230 nm. The percentage of H_2O_2 scavenging was calculated using Equation (S1). The maximum H_2O_2 scavenging was 83% for both SNP-Cd and SNP-Nb at 100 µg/mL. The IC_{50} value was 29.03 µg/mL for SNP-Cd

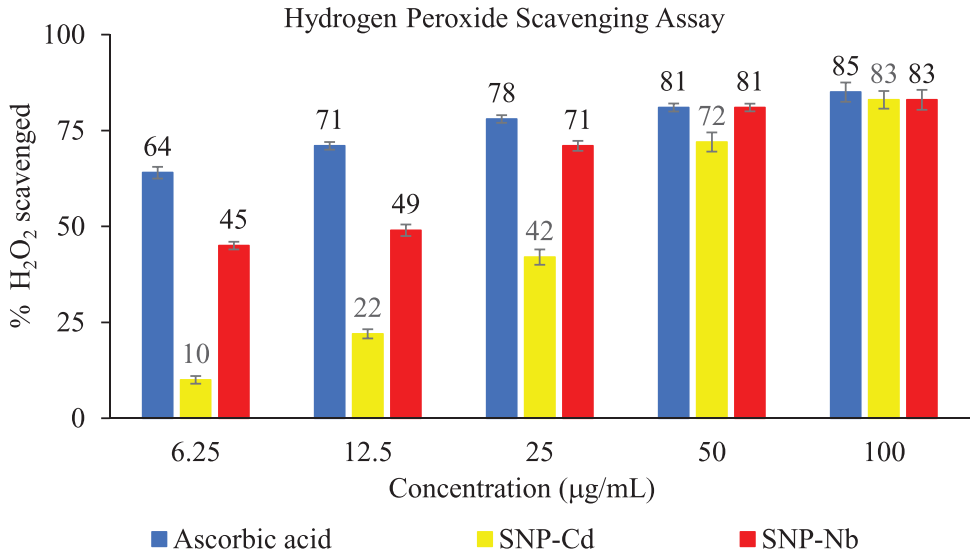


FIGURE 9 | Hydrogen peroxide scavenging assay for SNP-Cd and SNP-Nb. SNP-Cd, *C. dentatus* SNP; SNP-Nb, *C. dentatus* SNP.

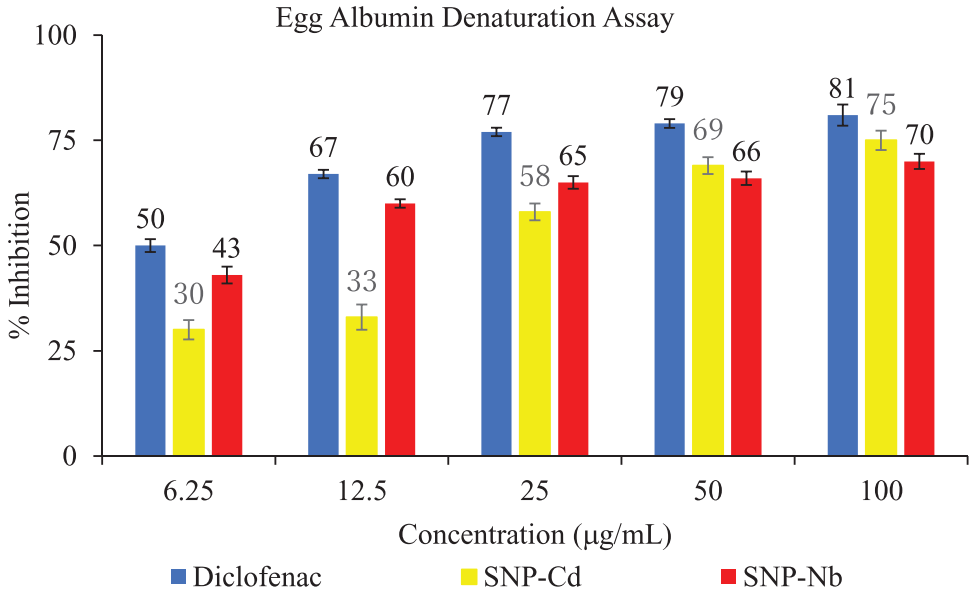


FIGURE 10 | Albumin denaturation assay for SNP-Cd and SNP-Nb. SNP-Cd, *C. dentatus* SNP; SNP-Nb, *C. dentatus* SNP.

and 9.07 µg/mL for SNP-Nb. The ascorbic acid IC_{50} value was 0.80 µg/mL. The results were dose dependent, and the differences were significant ($p < 0.05$).

The anti-inflammatory activity of the SNPs was also examined using the heat-induced egg albumin denaturation method, as described in previous reports [18]. This method assesses the ability of SNPs to prevent protein denaturation or protein tertiary or secondary structure disorientation. All the concentrations tested (100−6.25 µg/mL) significantly inhibited the denaturation of egg albumin in a concentration-dependent manner (Figure 10). The maximum inhibition was 75% for SNP-Cd and 70% for SNP-Nb at a concentration of 100 µg/mL. Diclofenac was used as a standard drug and exhibited inhibition of 81% at 100 µg/mL and an IC_{50} of 3.56 µg/mL. The IC_{50} of SNP-Cd was 21.20 µg/mL, and the IC_{50} of SNP-Nb was 7.18 µg/mL. The results were dose dependent, and the differences were significant ($p < 0.05$).

In this study, aqueous extracts of fronds of the ferns *C. dentatus* and *N. biserrata* were prepared and used for SNP synthesis. The formation of SNPs was preliminarily confirmed by a change in the color of the solution from light green or yellow to brown, and this color change was faster for SNP-Cd than SNP-Nb, due to their secondary metabolites responsible for the reduction of Ag(I) to Ag(0), as described in other reports (Figure S5) [8, 9].

The SPR at 420 nm for SNP-Cd was first observed with an accelerated color change after the mixing of the plant extracts and the $AgNO_3$ solution. The UV-Vis spectra for the SNP samples were narrow, thus indicating a small particle size distribution [19].

IR spectroscopy can be used to elucidate the physicochemical characteristics of materials and the mechanism of their

interaction with other molecules [20]. The peaks at 2843 and 2917 cm^{-1} for SNP-Cd, assigned to C-H and C-C vibrations, were not observed for SNP-Nb. Strong bands were observed at 1549 and 1273 cm^{-1} for SNP-Cd, whereas moderate to weak bands at 1558 and 1260 cm^{-1} were observed for SNP-Nb indicating N-O and C-O vibrations. These results could indicate the presence of highly electronegative elements or functional groups that are responsible for accelerated SNP-Cd formation, further confirming the results of visual color monitoring and UV-Vis analysis. Additional bands in the fingerprinting regions illustrate possible molecules that are involved in the synthesis of SNPs or that act as capping agents.

XRD patterns can be used to identify the crystalline substance known as the phase. In the present study, a wider FWHM corresponded to a smaller SNP size. The crystallite size of Ag was almost the same for the ferns *C. dentatus* (18.62 nm) and *N. biserrata* (22.02 nm). In contrast, the crystallite size of AgCl for *C. dentatus* (35.92 nm) was approximately three times larger than that for *N. biserrata* (13.50 nm). Meanwhile, the phytochemical composition influences the efficiency of the plant extracts in forming desired nanoparticles types or sizes with morphological properties are influenced by several aspects such as pH, synthesis temperature, extract concentration and volume [7, 18]. The purity of the formed Ag and AgCl nanoparticles was confirmed by their limited appearance on diffractograms. The Ag content was higher for both systems (67% for SNP-Cd and 68% for SNP-Nb) compared to the AgCl content which can explain the low amount of Cl from the EDS measurement Table S4.

DLS spectroscopy gave a moderate polydispersity (PDI) of 0.415 and a hydrodynamic particle size of 65.15 nm for SNP-Nbs. The PDI or dispersity based on the IUPAC measures the distribution of particle size population within a sample and ranges from zero (a perfect uniform sample) to one (perfect polydisperse samples with multiple size populations) [21, 22]. The hydrodynamic particle size was larger than the XRD crystallite size (Ag = 22.02 nm) due to the fern metabolites and solvent molecules bound to the central metal or because of Brownian motion, as previously reported [23]. SEM image confirmed aggregates of spherical formed SNP-Nb.

The application of nanoparticles for diagnostic, therapeutic, and drug delivery purposes has markedly impacted clinical therapeutics in the last two decades. Compared with conventional therapeutic agents, nanoscale drug carriers exhibit enhanced permeability and retention effects [23, 24]. Among the numerous drug delivery systems available, SNPs are used as a novel platform for a variety of therapeutic purposes due to their small particle size and large surface area [25]. In this study, fern-derived nanometric SNPs were investigated for their antioxidant and anti-inflammatory activities.

As summarized in Table S5, phosphomolybdenum reduction and H_2O_2 scavenging assays indicated excellent percent inhibition and IC_{50} values compared with the positive reference substance, ascorbic acid. These data confirmed that the synthesized SNPs are potential antioxidant agents capable of terminating radical chain reactions in diseases in which oxidative stress induced by reactive oxygen and nitrogen species overload is the major contributor [18]. The SNP-Cd with a slightly smaller Ag crystallite size and a larger AgCl crystallite size than SNP-Nb, gave a better phosphomolybdenum reduction activity, contrary to their H_2O_2 scavenging assays. So, particles sizes are not the only important factor for the activity of the SNPs. Moreover, the phytochemical constituents of the extracts used for their synthesis are equally important for their antioxidant activities. For example, in previous investigations, a high total phenolic content (127.28 ± 1.57 mg gallic acid equivalent per gram) of the methanol extract of *N. biserrata* was the major contributor to the depletion of alanine amino transferase and aspartate amino transferase, the reduced extent of malondialdehyde, the increased level of reduced glutathione, and elevated activities of some enzymes (e.g., catalase, glutathione reductase, glutathione peroxidase, glucose 6-phosphate dehydrogenase, glutathione S-transferase, and quinone reductase). Therefore, the phenolics, flavonoids and proteins present in this ferns contributes highly to their antioxidant activities [3–5].

Egg albumin denaturation anti-inflammation assays of the SNPs indicated excellent anti-inflammation potential, with IC_{50} values comparable to the non-steroidal anti-inflammatory drug diclofenac. A previous study reported that partitioned ethanolic extracts of *N. biserrata* inhibit the pro-inflammatory enzymes 15-lipoxygenase and cyclooxygenase-2 (COX-2) [26]. Ferns possesses a wide array of secondary metabolites like flavonoids, polyphenols and alkaloids which are essential source for developing anti-inflammatory agents. The chemical analysis of these compounds for *C. dentatus* and *N. biserrata* is limited. The SNP-Cd with a slightly smaller Ag crystallite size and larger AgCl crystallite size than SNP-Nb gave a better anti-inflammatory activity. As SNPs have a large surface area to volume ratio, it is suggested that they are better at blocking the activity of pro-inflammatory cytokines and inflammation-related enzymes compared with bulk samples. SNPs suppress the production of pro-inflammatory cytokines such as interleukin-12 and tumor necrosis factor-α and bring about a reduction in COX-2 gene expression at higher concentrations, which highlights their anti-inflammatory potential [27]. To the best of our knowledge and from a survey of the available literature, this work represents, for the first time, to characterize greenly synthesized SNPs using the ferns *C. dentatus* and *N. biserrata* and to examine their antioxidant and anti-inflammatory potential.

3 | Conclusions

In summary, SNPs were synthesized, for the first time, from aqueous extracts of *C. dentatus* and *N. biserrata* through green process. Aqueous extracts of fern fronds contained various compounds that act as reducing, capping, or stabilizing agents for SNP formation. The resulting SNPs were spherical, aggregated, and exhibited different sizes, as confirmed by XRD, SEM, and DLS analyses. Moreover, the antioxidant and anti-inflammatory potencies of the SNPs were assessed, and the results indicated their effectiveness against free radicals or oxidizing agents and highlighted their potential as anti-inflammatory agents, especially for the alleviation of age-associated oxidative stress, and inflammation pathologies. The present study thus demonstrated the potential pharmaceutical usages of SNP-Cd and SNP-Nb as the basis for future novel, effective, and safe antioxidant, and anti-inflammatory medications.

Conflicts of Interest

The authors declare no conflicts of interest.

Data Availability Statement

Data are available in the article's supplementary material.

References

1. A. Gurib-Fakim, "Medicinal Plants: Traditions of Yesterday and Drugs of Tomorrow," *Molecular Aspects of Medicine* 27 (2006): 1–93.

2. P. H. Lee, Y. M. Huang, and W. L. Chiou, "Fern Phenology," in *Current Advances in Fern Research*, ed. H. Fernández (Cham, Switzerland: Springer, 2019), 381.

3. R. Feng, C. Wei, S. Tu, F. Wu, and L. Yang, "Antimony Accumulation and Antioxidative Responses in Four Fern Plants," *Plant and Soil* 317 (2008): 93–101.

4. M. D. Shah, C. Gnanaraj, A. T. M. Emdadul Haque, and M. Iqbal, "Antioxidative and Chemopreventive Effects of *Nephrolepis biserrata* Against Carbon Tetrachloride (CCl_4)-induced Oxidative Stress and Hepatic Dysfunction in Rats," *Pharmaceutical Biology* 53 (2015): 31–39.

5. S. Singh, "Evaluation of In-Vitro Antioxidant Potential and Antimicrobial Activity of *Nephrolepis biserrata* (sw.) Schott. Leaf Extracts," *Anti-Infective Agents* 20 (2022): e010522204320.

6. A. K. Mittal, Y. Chisti, and U. C. Banerjee, "Synthesis of Metallic Nanoparticles Using Plant Extracts," *Biotechnology Advances* 31 (2013): 346–356.

7. C. Vanlalveni, S. Lallianrawna, A. Biswas, M. Selvaraj, B. Changmai, and S. L. Rokhum, "Green Synthesis of Silver Nanoparticles Using Plant Extracts and Their Antimicrobial Activities: A Review of Recent Literature," *RSC Advances* 11 (2021): 2804–2837.

8. C. N. Chick, T. Misawa-Suzuki, Y. Suzuki, and T. Usuki, "Preparation and Antioxidant Study of Silver Nanoparticles of *Microsorum pteropus* Methanol Extract," *Bioorganic & Medicinal Chemistry Letters* 30 (2020): 127526.

9. L. P. Luhata, C. N. Chick, N. Mori, et al., "Synthesis and Antioxidant Activity of Silver Nanoparticles Using the *Odontonema strictum* Leaf Extract," *Molecules* 27 (2022): 3210.

10. N. Assad, M. Naeem-ul-Hassan, M. Ajaz Hussain, et al., "Diffused Sunlight Assisted Green Synthesis of Silver Nanoparticles Using Cotoneaster Nummularia Polar Extract for Antimicrobial and Wound Healing Applications," *Natural Product Research* 25 (2023): 1–15.

11. S. Ullah, R. Khalid, M. F. Rehman, et al., "Biosynthesis of Phyto-Functionalized Silver Nanoparticles Using Olive Fruit Extract and Evaluation of Their Antibacterial and Antioxidant Properties," *Frontiers in Chemistry* 11 (2023): 1202252.

12. V. M. Bogatyrov, V. M. Gun'ko, M. V. Galaburda, et al., "The Effect of Photoactivated Transformations of Ag^+ and Ag^0 in Silica Fillers on Their Biocidal Activity," *Research on Chemical Intermediates* 45 (2019): 3985–4001.

13. S. Li, Y. Shen, A. Xie, et al., "Green Synthesis of Silver Nanoparticles Using *Capsicum Annuum* L. extract," *Green Chemistry* 9 (2007): 852–858.

14. C. G. Kumar and S. K. Mamidyala, "Extracellular Synthesis of Silver Nanoparticles Using Culture Supernatant of *Pseudomonas aeruginosa*," *Colloids and Surfaces B* 84 (2011): 462–466.

15. S. S. Shankar, A. Rai, A. Ahmad, and M. Sastry, "Rapid Synthesis of Au, Ag, and Bimetallic Au Core–Ag Shell Nanoparticles Using Neem (*Azadirachta indica*) Leaf Broth," *Journal of Colloid and Interface Science* 275 (2004): 496–502.

16. A. Jabbar, A. Abbas, N. Assad, et al., "A Highly Selective Hg^{2+} Colorimetric Sensor and Antimicrobial Agent Based on Green Synthesized Silver Nanoparticles Using *Equisetum diffusum* Extract," *RSC Advances* 13 (2023): 28666–28675.

17. F. E. A. Meva, J. O. A. Mbeng, C. O. Ebongue, et al., "*Stachytarpheta Cayennensis* Aqueous Extract, a New Bioreactor Towards Silver Nanoparticles for Biomedical Applications," *Journal of Biomaterials and Nanobiotechnology* 10 (2019): 102–119.

18. M. Raza, Z. Kanwal, A. Rauf, A. Sabri, S. Riaz, and S. Naseem, "Size- and Shape-Dependent Antibacterial Studies of Silver Nanoparticles Synthesized by Wet Chemical Routes," *Nanomaterials* 6 (2016): 74.

19. K. I. Hadjiivanov, D. A. Panayotov, M. Y. Mihaylov, et al., "Power of Infrared and Raman Spectroscopies to Characterize Metal-Organic Frameworks and Investigate Their Interaction With Guest Molecules," *Chemical Reviews* 121 (2020): 1286–1424.

20. L. P. Luhata, Y. Iizuka, R. Eda, et al., "Synthesis and Property of Silver Nanoparticles with Verbascoside," *Chemistry Letters* 53 (2023): upad024.

21. S. Das and A. Chaudhury, "Recent Advances in Lipid Nanoparticle Formulations with Solid Matrix for Oral Drug Delivery," *AAPS Pharm Sci Tech* 12 (2011): 62–76.

22. P. A. Hassan, S. Rana, and G. Verma, "Making Sense of Brownian Motion: Colloid Characterization by Dynamic Light Scattering," *Langmuir: The ACS Journal of Surfaces and Colloids* 31 (2014): 3–12.

23. H. Kobayashi and P. L. Choyke, "Super Enhanced Permeability and Retention (SUPR) Effects in Tumors Following Near Infrared Photoimmunotherapy," *Nanoscale* 8 (2016): 12504–12509.

24. D. Kovács, N. Igaz, M. K. Gopisetty, and M. Kiricsi, "Cancer Therapy by Silver Nanoparticles: Fiction or Reality?," *International Journal of Molecular Sciences* 23 (2022): 839.

25. F. Trotta, A. Dony, M. Mok, et al., "In Vitro Characterization of Bionanocomposites with Green Silver Nanoparticles: A Step towards Sustainable Wound Healing Materials," *Nano Select* 5 (2023): 2300087.

26. M. G. Aileen, T. Edsel, A. M. Rainear, et al., "In Vitro Anti-inflammatory Activity of *Nephrolepis biserrata* (Sw.) Schott Rhizome and Angiopteris palmiformis (Cav.) C. Chr. Leaf Extracts," *International Journal of Biosciences* 21 (2022): 279.

27. H. Agarwal, A. Nakara, and V. K. Shanmugam, "Anti-inflammatory Mechanism of Various Metal and Metal Oxide Nanoparticles Synthesized Using Plant Extracts: A Review," *Biomedicine & Pharmacotherapy* 109 (2019): 2561–2572.

Supporting Information

Additional supporting information can be found online in the Supporting Information section.